A Search for Dark Matter Annihilation
with the Whipple 10m Telescope

M. Wood[1], G. Blaylock[2], S. M. Bradbury[3], J. H. Buckley[4], K. L. Byrum[5], Y. C. K. Chow[1], W. Cui[6], I. de la Calle Perez[7], A. D. Falcone[8], S. J. Fegan[1], J. P. Finley[6], J. Grube[3], J. Hall[9], D. Hanna[10], J. Holder[11], D. Horan[5], T. B. Humensky[12], D. B. Kieda[13], J. Kildea[14], A. Konopelko[6], H. Krawczynski[4], F. Krennrich[15], M. J. Lang[16], S. LeBohec[13], T. Nagai[15], R. A. Ong[1], J. S. Perkins[14], M. Pohl[15], J. Quinn[17], H. J. Rose[3], G. H. Sembroski[6], V. V. Vassiliev[1], R. G. Wagner[5], S. P. Wakely[12], T. C. Weekes[14], and A. Weinstein[1]

mdwood@astro.ucla.edu

vvv@astro.ucla.edu

ABSTRACT

[1]Department of Physics and Astronomy, University of California, Los Angeles, CA 90095, USA

[2]Department of Physics, University of Massachussetts, Amherst, MA 01003-4525, USA

[3]School of Physics and Astronomy, University of Leeds, Leeds, LS2 9JT, UK

[4]Department of Physics, Washington University, St. Louis, MO 63130, USA

[5]Argonne National Laboratory, 9700 S. Cass Avenue, Argonne, IL 60439, USA

[6]Department of Physics, Purdue University, West Lafayette, IN 47907, USA

[7]Department of Physics, University of Oxford, Oxford, OX1 3RH, UK

[8]Department of Astronomy and Astrophysics, 525 Davey Lab.,Penn. State University, University Park, PA 16802, USA

[9]Fermi National Accelerator Laboratory, Batavia, IL 60510, USA

[10]Physics Department, McGill University, Montreal, QC H3A 2T8, Canada

[11]Department of Physics and Astronomy, University of Delaware, Sharp Laboratory, Newark, DE 19716, USA

[12]Enrico Fermi Institute, University of Chicago, Chicago, IL 60637, USA

[13]Physics Department, University of Utah, Salt Lake City, UT 84112, USA

[14]Fred Lawrence Whipple Observatory, Harvard-Smithsonian Center for Astrophysics, Amado, AZ 85645, USA

[15]Department of Physics and Astronomy, Iowa State University, Ames, IA 50011, USA

[16]Physics Department, National University of Ireland, Galway, Ireland

[17]School of Physics, University College Dublin, Belfield, Dublin 4, Ireland

We present observations of the dwarf galaxies Draco and Ursa Minor, the local group galaxies M32 and M33, and the globular cluster M15 conducted with the Whipple 10m gamma-ray telescope to search for the gamma-ray signature of self-annihilating weakly interacting massive particles (WIMPs) which may constitute astrophysical dark matter (DM). We review the motivations for selecting these sources based on their unique astrophysical environments and report the results of the data analysis which produced upper limits on excess rate of gamma rays for each source. We consider models for the DM distribution in each source based on the available observational constraints and discuss possible scenarios for the enhancement of the gamma-ray luminosity. Limits on the thermally averaged product of the total self-annihilation cross section and velocity of the WIMP, $\langle \sigma v \rangle$, are derived using conservative estimates for the magnitude of the astrophysical contribution to the gamma-ray flux. Although these limits do not constrain predictions from the currently favored theoretical models of supersymmetry (SUSY), future observations with VERITAS will probe a larger region of the WIMP parameter phase space, $\langle \sigma v \rangle$ and WIMP particle mass (m_χ).

Subject headings: gamma rays: observations — dark matter

1. Introduction

The existence of dark matter (DM) is supported by a variety of observational data including measurements of the cosmic microwave background (Spergel et al. 2007), the large-scale distribution of galaxies (Tegmark et al. 2004), and gravitational lensing (Clowe et al. 2006). In the ΛCDM cosmological model that is currently favored by these data, DM comprises approximately $\sim 26\%$ of the total energy density of the universe (Spergel et al. 2007). However, the nature of the particles that constitute DM remains unknown. A popular DM candidate is weakly interacting massive particles (WIMPs), which existed in thermal equilibrium during the early universe and later decoupled as the universe expanded. Since the time of decoupling, the WIMPs have remained non-relativistic, behaving as a collisionless fluid on all but perhaps the shortest spatial scales. In order to reproduce the observed relic density of DM, this hypothetical particle would need to have a cross section on the scale of weak interactions. A stable particle with these properties, the lightest neutralino χ, can be accommodated in theories of supersymmetry (SUSY).

The mass of the neutralino is constrained to be $\gtrsim 6$ GeV by CMB measurements and accelerator searches (Bottino et al. 2003) and $\lesssim 100$ TeV by the unitarity limit on the thermal relic (Griest & Kamionkowski 1990). In the conventional SUSY scenarios, the neu-

tralino is a Majorana particle which can efficiently self-annihilate in astrophysical environments with high DM density producing secondary particles including high-energy gamma rays. The former and current generation of Air-Cherenkov Telescopes (ACTs), including Whipple, HEGRA, CANGAROO-III, VERITAS, H.E.S.S., and MAGIC are sensitive in the gamma-ray energy range from below 100 GeV to above 10 TeV and can therefore make a substantial contribution to the search for the signatures of DM self-annihilation. Recently several ACTs have detected gamma rays from the Galactic Center (G.C.) (Albert et al. 2006; Aharonian et al. 2004; Kosack et al. 2004). Although a more traditional astrophysical origin for this signal is currently favored (Atoyan & Dermer 2004; Aharonian & Neronov 2005), DM self-annihilation has been proposed as a possible explanation for these observations (Horns 2005).

We present observations taken with the Whipple 10m telescope of five astrophysical sources with the purpose of detecting the signature of DM self-annihilation. Section 2 summarizes the motivations for selecting each source. In Section 3 we discuss the signature of DM self-annihilation into gamma rays and its dependence on the source astrophysics and the particle physics properties of the WIMP. In Section 4 we review the atmospheric Cherenkov technique and the methods used to analyze the data. Results of the data analysis are described in Section 4.3. Models for the DM distribution and scenarios for the enhancement of the gamma-ray flux are presented in Section 5. We conclude in Section 6 by discussing the implications of these observations for the parameter space of allowed SUSY models.

2. Review of Observational Targets

Because the gamma-ray signature of the neutralino is proportional to the square of the local density, the spatial scales that contribute to the total gamma-ray flux from a DM halo are much smaller than the spatial scales contributing to the halo mass. On these small spatial scales, the evolution of DM is typically driven by its interaction with baryonic matter, which dominates the gravitational potential. The influence of baryons in the form of dense stellar populations, molecular clouds, and central black holes could potentially lead to a much higher central DM concentration than that inferred from the large-scale DM distribution and thus substantially enhance the annihilation signal. Therefore it is attractive to consider sources that represent a diverse set of astrophysical environments, which could boost the gamma-ray luminosity. We have selected the dwarf galaxies Draco and Ursa Minor, the local group galaxies M32 and M33, and the globular cluster M15 for observations with the Whipple 10m telescope based on the analysis of observational data and various potential scenarios for DM enhancement in these objects.

2.1. Draco and Ursa Minor

Dwarf spheroidal galaxies have attracted considerable theoretical attention as potential DM annihilation gamma-ray sources (Baltz et al. 2000; Tyler 2002; Strigari et al. 2007; Bergström & Hooper 2006; Colafrancesco et al. 2007) due to their large observed mass-to-light ratios (M/L). Studies of surface brightness morphology have found a smooth symmetrical profile in the core of Draco (Piatek et al. 2002; Ségall et al. 2007) but significant structure in the central regions of Ursa Minor (Bellazzini et al. 2002), which may be indicative of tidal interaction with the Milky Way. The observed stellar velocity dispersions in Draco and Ursa Minor imply that the dynamics of these systems are dominated by DM on all spatial scales and provide robust lower bounds on the astrophysical contribution to the gamma-ray flux in these systems.

Both Draco and Ursa Minor possess low metallicity stellar populations with an age of $\sim$10 Gyr (Aparicio et al. 2001; Shetrone et al. 2001). The absence of recent star formation suggests that neither system has undergone a significant merger or accretion event since this early star formation epoch. Furthermore, because the two-body relaxation time in these galaxies significantly exceeds the Hubble time, it is unlikely that baryonic matter played a significant role in shaping the present-day DM distribution. Therefore primordial DM fluctuations formed on small spatial scales during initial violent relaxation could have been preserved and may boost the gamma-ray flux from these objects.

2.2. M15

Although there is no observational evidence for the presence of significant DM in globular clusters, the association of globular clusters and DM halos fits naturally into the standard paradigm of hierarchical structure formation. In the primordial formation scenario proposed by Peebles (1984), globular clusters are formed in DM overdensities in the early universe and may therefore retain a significant fraction of this primordial halo in the current epoch. Given that the extremely dense stellar cores of globular clusters dominate the gravitational potential of these systems, the observable effects of an extended DM halo may be minimal. Moore (1996) argued that the presence of tidal tails in some globular clusters suggests that globular clusters are not embedded in DM halos. Recent simulations (Mashchenko & Sills 2005a,b; Saitoh et al. 2006) have challenged this picture, showing that an extended halo may be compatible with the observable properties of globular clusters, although much of the original halo mass could be stripped by tidal interactions with the host galaxy.

The proximity and potentially high central DM density of M15 favor this source for

indirect DM searches. With a core radius of ∼0.2 pc and extreme central density in excess of 10^7 $M_\odot$ pc^{-3} (Dull et al. 1997), M15 is the prototype for the core-collapsed globular cluster. During core collapse, the globular cluster is predicted to relax through stellar two-body collisions to a power-law density profile that extends down to the smallest observable scales (Binney & Tremaine 1987). If M15 was originally embedded in a DM halo, this evolutionary process must significantly compress the central DM distribution and dramatically enhance the gamma-ray flux. However, the poorly understood process of kinetic heating of DM in the core of the cluster by stars and hard binaries could lead to a depletion of DM from this region.

2.3.   M32

The model for compression of DM through the gravitational contraction of dense stellar populations may also apply on the galactic scale. M32 is the closest compact elliptical galaxy and may have formed in a merging event between M31 and a low-luminosity spiral galaxy (Bekki et al. 2001) in which the disk component of M32 was tidally stripped. Stellar kinematical data strongly support the presence of a single supermassive compact object in the center of the galaxy with a mass of 2–4 × 10^6 $M_\odot$ (Joseph et al. 2001). The core of M32 has a relatively homogeneous stellar population with an intermediate age of approximately 4 Gyr (Corbin et al. 2001; del Burgo et al. 2001). Lauer et al. (1998) estimate M32's core relaxation time scale to be 2–3 Gyr, implying that the nucleus of M32 had at least a few relaxation times to evolve since the last significant merging event. Such events in which a massive black hole binary is formed are predicted to deplete the central density by evacuating stars and destroying any potential DM cusp in the galaxy core (Milosavljević et al. 2002). Collisional two-body relaxation of a stellar population around a black hole is analytically predicted to result in a steady state power-law stellar density profile with power-law index between 3/2 and 7/4 (Bahcall & Wolf 1976). Optical and infrared data indicate a stellar density profile compatible with a power-law index in the range 1.4–1.9 at the resolution limit of 0.07 pc (Corbin et al. 2001; Lauer et al. 1998). Because the condensation of baryons in galactic nuclei may greatly enhance the central concentration of DM halos, the stellar density in the core of M32, in excess of 10^7 $M_\odot$ pc^{-3} and the highest known among nearby systems (Lauer et al. 1998), makes it a promising candidate for the detection of DM annihilation.

2.4. M33

By observing astrophysical systems capable of rapid evolution, one may be able to overcome dynamical limitations on the neutralino annihilation rate, if it is limited by the scattering of WIMPs into a very small annihilation region in the galactic nucleus. M33 is remarkable for the small relaxation time, $\sim$3 Myr, in its stellar nucleus of approximately 0.2 pc, which results from the high stellar density , 5×10^6 M$_\odot$ pc^{-3}, and extremely low velocity dispersion, 21 km s^{-1}, in this region (Lauer et al. 1998). M33 is a low-luminosity, DM dominated, bulgeless spiral galaxy with a dark halo mass of approximately 5.1×10^{11} M$_\odot$ (Corbelli & Salucci 2000). The mass of the black hole in its center is less than 1.5×10^3 M$_\odot$ (Gebhardt et al. 2001; Merritt et al. 2001). The stellar population in the nucleus of M33 can be modeled by two bursts of star formation 2 and 0.5 Gyr ago suggesting the possibility of a merger in the last $\sim$Gyr. However, due to its rapid collisional relaxation time, M33 could have developed a core-collapsed nucleus in the period since the last merging event.

3. DM Annihilation Flux

The differential flux of gamma rays from WIMP annihilation along a line of sight is given by

$$\frac{d\phi(\vec{\psi}, \Delta\Omega)}{dE} = \frac{\langle\sigma v\rangle}{8\pi m_\chi^2} \left(\frac{dN(E, m_\chi)}{dE}\right) \int_{\Delta\Omega} d\Omega \int \rho^2\left(s, \vec{\psi}, \Omega\right) ds, \tag{1}$$

where ρ is the DM mass density, m_χ is the mass of the WIMP particle, $\langle\sigma v\rangle$ is the thermally averaged product of the total self-annihilation cross section and the velocity of the WIMP, $dN(E, m_\chi)/dE$ is the differential yield per annihilation, $\Delta\Omega$ is the solid angle observed, and $\vec{\psi}$ is the direction of the line of sight integration.

This expression can be factored as

$$\frac{d\phi(\vec{\psi}, \Delta\Omega)}{dE} = \phi_{1\%} \left(\frac{\langle\sigma v\rangle}{3 \times 10^{-26} \text{ cm}^3 \text{ s}^{-1}}\right)$$
$$\times \left(\frac{100 \text{ GeV}}{m_\chi}\right)^2 \left(\frac{dN(E, m_\chi)/dE}{10^{-2} \text{ GeV}^{-1}}\right) \frac{J(\vec{\psi}, \Delta\Omega)}{1.45 \times 10^4}, \tag{2}$$

where $\phi_{1\%} = 6.64 \times 10^{-12}$ cm^{-2} s^{-1} is 1% of the integral Crab Nebula flux above 100 GeV as extrapolated from the power-law fit of 3.2×10^{-11} (E/TeV)$^{-2.49}$ cm^{-2} s^{-1} TeV^{-1} reported by Hillas et al. (1998). Following Bergström et al. (1998), the astrophysical component, which depends on the DM density profile, is expressed in terms of the dimensionless quantity J,

$$J(\vec{\psi}, \Delta\Omega) = \left(\frac{1}{\rho_c^2 R_H}\right) \int_{\Delta\Omega} d\Omega \int \rho^2\left(s, \vec{\psi}, \Omega\right) ds, \tag{3}$$

which we normalized to the critical density $\rho_c = 9.74 \times 10^{-30}$ g cm^{-3} and the Hubble radius $R_H = 4.16$ Gpc.

3.1. DM Halo Profiles

Estimation of J for a particular astrophysical object critically depends on the DM density profile. Numerical cold dark matter (CDM) simulations, applicable in the regions where DM dominates the overall gravitational potential, indicate the existence of a universal density profile across the spectrum of halo masses, from dwarf galaxies to galaxy clusters, which can be fit by,

$$\rho(r) = \rho_s \left(\frac{r}{r_s}\right)^{-\gamma} \left(1 + \left(\frac{r}{r_s}\right)^{\alpha}\right)^{-\frac{\beta-\gamma}{\alpha}}. \tag{4}$$

Simulations have consistently found that the large-scale ($r \gg r_s$) asymptotic behavior is compatible with $\beta \simeq 3$. The value of the inner logarithmic slope, γ, is less certain due to numerical resolution effects at the smallest scales. The so-called NFW profile, $(\alpha,\beta,\gamma) = (1,3,1)$, (Navarro et al. 1996) has an inner asymptotic of r^{-1}. Profiles with a steeper inner power-law cusp, $(\alpha,\beta,\gamma) = (1.5,3,1.5)$, have also been suggested (Moore et al. 1999). Recent high-resolution simulations have pointed to an intermediate value for the inner power-law cusp $\gamma \sim 1.2$ (Diemand et al. 2005) and a possible asymptotic shallowing approaching smaller scales (Navarro et al. 2004; Merritt et al. 2006).

The density profiles of simulated DM halos can described by their virial mass m_{vir} and concentration c, which are related to ρ_s and r_s. Using a sample of simulated DM halos with masses 10^{11}–10^{14} h^{-1} M$_\odot$, Bullock et al. (2001) found that the median halo concentration at $z = 0$ is correlated with virial mass and can be well approximated by the expression,

$$c = 9 \left(\frac{m_{vir}}{1.5 \times 10^{13} h^{-1} M_\odot}\right)^{-0.13}, \tag{5}$$

with a scatter of $\Delta \log c \simeq 0.14$.

Observations of low surface brightness galaxies (de Blok et al. 2001) have motivated an alternative form for the halo density profile which fits the rotation curves of these galaxies,

$$\rho(r) = \rho_s \left(1 + \frac{r}{r_s}\right)^{-\gamma} \left(1 + \left(\frac{r}{r_s}\right)^{\alpha}\right)^{-\frac{\beta-\gamma}{\alpha}}. \tag{6}$$

A specific choice of $(\alpha,\beta,\gamma) = (2,3,1)$ is known as the Burkert profile (Burkert 1995). Given the present state of uncertainty regarding the inner shape of DM halos, we use both the NFW

and Burkert profiles as representative of the possible range of inner density asymptotes in DM dominated halos.

The existence of DM halo substructures is a central prediction of CDM cosmology and may significantly enhance the DM annihilation flux as compared to that predicted for a smooth halo. Numerical simulations have predicted that these substructures have a power-law mass function $dN/dM \sim M^{-\alpha}$ with $\alpha \simeq 2$ (Diemand et al. 2006). The mass spectrum cutoff, m_0, for these structures is set by the free streaming and collisional damping length scales in the early universe and depends on the microphysical properties of the neutralino. A neutralino with mass $m_\chi = 100$ GeV is estimated to have $m_0 \sim 10^{-6}$ $M_\odot$ (Green et al. 2005). The abundance of these substructures at $z = 0$ is uncertain and depends on the fraction that survive disruption during the hierarchical merger and accretion processes. Current CDM simulations do not have sufficient resolution to model explicitly the mass function at all relevant scales. A recent estimate of the contribution of substructure to the DM annihilation flux places a lower limit on the enhancement to J relative to a smooth halo of 2–3 (Diemand et al. 2007). Strigari et al. (2007) obtain an upper bound of $\sim$100 on the substructure enhancement by summing the contribution of all substructures above $m_0 \simeq 10^{-5}$ $M_\odot$ and assuming a mass function with α=1.9.

In the galaxies in which baryonic matter dominates the mass profile in the central region, the observational constraints on the astrophysical enhancement J are weak. Due to the large concentration of baryonic matter on small scales, the evolution of DM in galactic nuclei is likely significantly affected by the gravitational interaction of neutralinos with a central black hole, high density stellar populations, and gas. Evolutionary condensation of baryons in the core of a DM halo gives rise to a DM density enhancement beyond what would be expected from the gravitational interaction of DM alone. Using CDM simulations that combined both dissipationless DM particles and a baryonic component composed of gas and stars, Gnedin et al. (2004) observed that baryon condensation increases the central concentration of a DM halo.

The adiabatic compression of DM in the core of a halo through the slow growth of a central black hole has been suggested as a mechanism for increasing the flux from DM self-annihilation (Gondolo & Silk 1999). However, the magnitude of this effect depends strongly on the ratio of the initial and final masses of the black hole, its initial alignment with the center of the DM halo, and the merging history of the galactic nucleus (Ullio et al. 2001). Merritt & Cruz (2001) have shown that a typical merger event between black holes of comparable mass destroys cuspy profiles. The effect of gravitational scattering of DM particles by infalling baryons in the central regions of galactic nuclei may also be significant. The transfer of momentum to the dark matter component in these interactions should lead

to the partial evaporation of DM from the center of the galaxy. The ejection of DM particles through the gravitational slingshot process in the vicinity of binaries will further enhance the DM outflow from the centers of galactic nuclei. It might be expected that for a variety of astrophysical objects the main contribution to J originates from the regions of high baryonic density. The diversity of conditions affecting the DM distribution in the core of a galactic nucleus (presence or absence of a black hole, stellar velocity dispersion, density of baryonic matter, merging history, etc.) argues for observations of a variety of astrophysical objects in which DM self-annihilation might be amplified due to the gravitational interaction with baryons.

3.2. DM Annihilation Spectrum

The differential yield of gamma-ray photons per neutralino self-annihilation is a sum over final-state contributions,

$$
\begin{aligned}
\frac{dN(E, m_\chi)}{dE} &= 2b_{\gamma\gamma}\delta\left(E - m_\chi\right) \\
&+ \sum_i b_{\gamma i}\delta\left(E - m_\chi + \frac{m_i^2}{4m_\chi}\right) + \sum_i b_i \frac{dN_i(E, m_\chi)}{dE},
\end{aligned} \tag{7}
$$

where b_X indicates the branching fraction of neutralino self-annihilation into a specific final-state channel X. The first two terms represent annihilations into mono-energetic photons through either one or two photon channels. The last term is a sum over all channels which contribute to the continuum flux, which arises primarily from the decay of π^0 mesons produced in the hadronization of the fermion and boson final states (for a review see Jungman et al. (1996)). The two-body annihilation modes into mono-energetic photons, $\gamma\gamma$ and $Z\gamma$, are significantly suppressed as compared to the continuum component, with branching ratios $\sim 10^{-2}$–10^{-3} (Bergström & Ullio 1997; Bergström et al. 1998).

The differential spectrum of the π^0 decay component is relatively featureless and similar for all channels. It falls exponentially at high energies terminating at m_χ where it is enhanced by internal bremsstrahlung from charged decay components (Birkedal et al. 2005), resulting in an edge-like feature at $E_\gamma = m_\chi$ (see Figure 1). Decays into all quark and bosonic states differ only slightly in the amplitudes of the π^0 and internal bremsstrahlung components. However, decay into τ leptons generates a significantly harder spectrum, due to direct production of π^0 mesons in processes such as $\tau^\pm \to \pi^\pm \pi^0 \nu$. In this work, the $b\bar{b}$ and $\tau^+\tau^-$ spectra are used to contrast the detection prospects in the case of a soft or hard neutralino self-annihilation spectrum, respectively.

Although observing regions of high baryonic density improves the chances of indirect
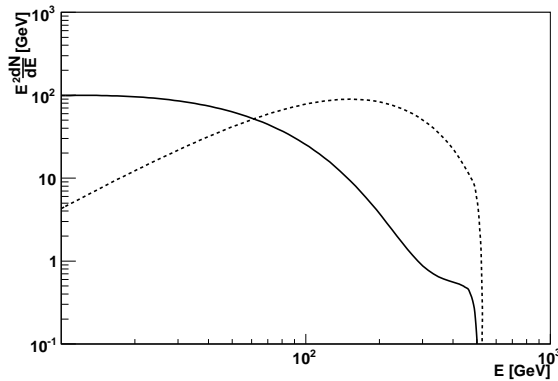
Fig. 1.— Spectral energy density per annihilation for a neutralino of mass 500 GeV annihilating to $b\bar{b}$ (solid line) and $\tau^+\tau^-$ (dashed line). These spectra were generated using the PYTHIA Monte Carlo package (Sjöstrand et al. 2001).

neutralino detection, the high density of baryonic matter comes with the price of potentially high astrophysical gamma-ray backgrounds. High-energy processes that take place in galactic nuclei, such as acceleration of particles in supernova shocks or the jets formed by accreting black holes, interactions of cosmic rays with molecular clouds, etc., can generate detectable gamma-ray fluxes from these regions. In these processes, particles producing gamma rays are most likely accelerated stochastically resulting in a power-law differential energy spectrum with index $\sim$2. The truncation of the spectrum of gamma rays from neutralino annihilation at the neutralino mass can, in principle, be mimicked by traditional astrophysical processes. For example, local absorption of gamma rays through pair production in high-density optical and infrared diffuse photon fields would cause an exponential cutoff in the spectrum. However, such truncation would depend on the specific properties of the source and would not be a common observational feature across multiple objects.

4. Observations and Analysis

The TeV gamma-ray observations of the five sources reported in this work were taken with the Whipple 10m telescope located at the Fred Lawrence Whipple Observatory in southern Arizona, USA. The telescope is equipped with a camera consisting of 379 photomultiplier tubes, covering a field of view of diameter $2.4°$, which detects the short-duration Cherenkov light flashes emitted by secondary particles generated in cosmic- and gamma-ray-induced atmospheric cascades. A detailed description of the telescope optics and camera configuration

is presented elsewhere (Kildea et al. 2007).

4.1. Observations

The five sources were observed over the course of four observing seasons using two different modes of operation: ON/OFF and TRACK. The ON/OFF mode is characterized by a sequential pair of 28 minute runs in which the ON run is obtained by pointing the telescope in the direction of the source and the OFF run is taken at the same azimuth and elevation but offset by 28 minutes in right ascension for background estimation. The ON/OFF technique minimizes systematic errors due to the changing state of the atmosphere and variations in the night-sky brightness. The TRACK mode observations are not followed by dedicated OFF observations. Instead, a contemporaneous but unrelated OFF run of similar elevation and average night-sky background noise is selected and then analyzed with the TRACK mode observation in the same way as the ON/OFF pair. To reduce systematic errors due to variations in the night-sky background between ON and OFF fields, artificial noise was injected on a pixel by pixel basis into either ON or OFF runs to equalize them (Weekes 1996). The total accumulated exposures in ON and TRACK modes and observation epochs for each source are summarized in Table 1.

4.2. Data Analysis

The light distributions of the Cherenkov images were parameterized using a standard moment analysis (Hillas 1985). The parameter *size* characterizes the total amount of light in the image while the parameters *width* and *length*, *distance*, and α describe the shape, location, and orientation of the image, respectively. A set of selection criteria, referred to as *Supercuts* (Reynolds et al. 1993), were used to select gamma-ray-like images with an efficiency of $\sim$50%, while rejecting >99% of cosmic rays.

For events passing the *Supercuts* criteria, a histogram of the α parameter is generated. Gamma-ray events originating from a source in the center of the field appear as an excess in the region of the α-histogram with $\alpha \leq 15°$. The residual background in the signal region of the ON-source observation is estimated from the number of events obtained from the same region of the OFF-source observation rescaled by the ratio of the OFF to ON livetimes. In the case of the TRACK mode observations, the background estimate from the matching OFF-source observation is scaled by an additional factor, equalizing backgrounds in a sideband region $20° < \alpha < 65°$ on a run-by-run basis. For each source, the significance of an excess

in the signal region is evaluated with the maximum likelihood method of Li & Ma (1983).

The method of analysis described estimates the integral gamma-ray excess which is the convolution of the effective area of the Whipple 10m telescope shown in Figure 2 with the spectrum of the source. The gamma-ray collecting area is nearly constant at $\sim 4 \times 10^8$ cm^2 for photon energies above 1 TeV and declines rapidly in the energy regime below ~ 400 GeV. The differential gamma-ray detection rate, the product of effective collecting area and source spectrum, is shown for a Crab Nebula-like spectrum in Figure 3. The peak of the detection rate is ~ 400 GeV and is a relatively weak function of the index of the power-law spectrum in the range ~ 2–3. Despite the fact that the continuum neutralino spectrum can not be approximated as a power law, for neutralino masses exceeding approximately 400 GeV the differential gamma-ray detection rate peaks in the vicinity of this energy as illustrated in Figure 3 for $m_\chi = 1$ TeV. Thus the integral constraints discussed in this paper are appropriate for a source with a neutralino-like spectrum as they have been optimized to produce the best sensitivity for the sources which peak in the energy range 300–400 GeV. The integral method remains applicable for neutralino masses below 400 GeV. However, the sensitivity deteriorates rapidly as the peak of the detection rate falls significantly below 400 GeV.

In this analysis we have not searched for the monoenergetic line feature of the neutralino self-annihilation spectrum. The Whipple 10m telescope has an energy resolution of $\sim 30\%$ which ultimately limits the sensitivity to monoenergetic photons. The search for the continuum component of the spectrum can provide an equivalent or better sensitivity to neutralino annihilations as compared to searching for the monoenergetic line given that under the preferred particle physics scenarios the branching ratios to two and one photon channels is less than one percent. A dedicated search for monoenergetic photons could be a goal of a refined analysis if an integral excess is detected.

The accuracy of the reconstruction of the arrival direction of individual photons for the Whipple 10m telescope for a source in the center of the field of view is a function of photon energy and changes from $\sim 20'$ at 300 GeV to $\sim 2'$ at 10 TeV. The event selection criterion $\alpha \leq 15°$ corresponds to an angular cut in the image plane of $\sim 15'$ which translates into a solid angle $\Delta \Omega$ of 6×10^{-5} sr which is used in the calculation of J (Equation 3).

The Crab Nebula is the standard calibration source for ground-based gamma-ray astronomy. Observations of the Crab Nebula were taken during the same four year period as the observations of the sources of interest. These data were analyzed with the same technique to calibrate the gamma-ray detection efficiency of the Whipple 10m telescope. The differential flux of the Crab nebula at 400 GeV is estimated using the spectral parameterization of Hillas et al. (1998). By scaling the observed gamma-ray rate from the putative

DM sources to the contemporaneous rate of the Crab Nebula, the systematics due to the changing performance of the telescope optics and camera system were corrected for.

4.3. Results

Using the *Supercuts* criteria, the excess gamma-ray rate and its significance for each source was calculated under the hypothesis of a point source in the center of the field of view. No significant excess was detected from any of the five sources observed (see Table 2). In the absence of a significant detection, the 95% C.L. upper limit on the rate from each source was calculated following the method of Helene (1983). The upper limit on the differential spectral energy density $E^2 dF/dE$ at 400 GeV is calculated for each source by scaling the gamma-ray rate to the observed Crab rate during the same observation epoch.

The 95% C.L. upper limits for all sources are 6–9% of the Crab Nebula flux with the exception of M15 for which the exposure time was significantly shorter. ACT observations of M32 were reported by the HEGRA collaboration (Aharonian et al. 2003). This work places a 99% C.L integral flux upper limit of 4.4% of the Crab Nebula rate for M32 which is compatible with the results presented in this work.

5. Analysis of Astrophysical Enhancement Factors

The primary difficulty in constraining the parameter space of allowable SUSY models is due to the significant uncertainty in the astrophysical enhancement factor, J (Equation 3). A lower bound on J can be estimated by extrapolating the DM density measured on large spatial scales ($r \gg r_s$) into the small scales (where most of the DM annihilation signal originates) by using a profile with a weak cusp (NFW) or central core (Burkert). However, for each of the sources considered there may exist astrophysical mechanisms which could enhance the density of DM in the core of the halo and boost the luminosity due to neutralino self-annihilation by several orders of magnitude. A discussion follows for each source which presents both a conservative estimate of J as well as possible scenarios for its enhancement which take into account the source's unique astrophysical environment.

5.1. Draco and Ursa Minor

Because the gravitational potentials of Draco and Ursa Minor are dominated by DM on all observationally resolved scales, studies of stellar kinematics in these systems provide

Table 1. Summary of observation period and exposure time for ON and TRACK
observing modes

Source	Period	ON Exposure (hours)	TRACK Exposure (hours)	Total Exposure (hours)
Draco	Mar 2003 - Jul 2003	7.4	6.9	14.3
Ursa Minor	Jan 2003 - Jul 2003	7.9	9.3	17.2
M32	Sep 2004 - Dec 2004	6.9	0	6.9
M33	Oct 2002 - Dec 2004	7.9	9.2	17.0
M15	Jun 2002 - Jul 2002	0.2	1.0	1.2

Table 2. Detected Gamma-ray rates, inferred upper limits on the gamma-ray rate,
significances, and differential gamma-ray flux upper limits

Source	Excess (γ min^{-1})	95% C.L. Upper Limit (γ min^{-1})	σ	$E^2\frac{dF}{dE}$ at 400 GeV Upper Limit (erg cm^{-2} s^{-1})	(% Crab)
Draco	0.001 ± 0.066	0.14	0.02	5.10×10^{-12}	6.23
Ursa Minor	0.075 ± 0.070	0.20	1.07	7.30×10^{-12}	8.94
M32	-0.240 ± 0.170	0.21	-1.44	6.00×10^{-12}	7.34
M33	-0.012 ± 0.085	0.16	-0.14	5.75×10^{-12}	7.04
M15	0.496 ± 0.269	0.94	1.80	2.68×10^{-11}	32.8

robust constraints on their DM density profiles at radii greater than $\sim$0.5 kpc. Strigari et al. (2007) have used the radial velocity data sets compiled by Wilkinson et al. (2004) and Muñoz et al. (2005) to derive constraints on the parameters r_s and ρ_s of their DM halos under the assumption that the DM follows an NFW density profile. The best-fit contours in the r_s–ρ_s plane are shown in Figures 4 and 6 for Draco and Ursa Minor, respectively. A similar analysis of the Draco data set by Mashchenko et al. (2006) which considered both NFW and Burkert DM density profiles obtained similar constraints on r_s and ρ_s, shown in Figures 4 and 5. Both analyses find a region of degeneracy in the r_s–ρ_s plane which is attributable to the weak constraints on the stellar velocity anisotropy. The region of degeneracy for these models, however, is nearly parallel to the isocontours of J which results in a much smaller uncertainty for this parameter. Conservative allowable ranges for J calculated using the mass models presented by Mashchenko et al. (2006) and Strigari et al. (2007) are summarized in Table 3.

The inner logarithmic slope (γ) of the DM density profile in Draco and Ursa Minor is not observationally constrained. A value of $\gamma > 1$ could potentially enhance by 2–3 orders of magnitude the value of J with respect to the estimates presented in Table 3. The presence of DM substructures is another potential factor contributing to the enhancement of J. Strigari et al. (2007) calculated an upper bound of $\sim$100 on the enhancement due to substructures for a generic DM halo. The distortion of the gravitational potential by DM substructures may be reflected in the distribution of stellar populations. Stellar lumps within the central 10 arc minutes of Ursa Minor have been detected, and the study of the stellar proper motion suggests that the lifetime of these structures should be no longer than $\sim$5 Myr (Eskridge & Schweitzer 2001). If proven statistically significant, these observations may indicate the existence of small scale substructures in the DM distribution. However a conventional astrophysical explanation such as the projection of a cold extratidal population of stars is also possible (Wilkinson et al. 2004).

5.2. M15

Models for the M/L of M15 are consistent with a purely baryonic mass profile (van den Bosch et al. 2006) and therefore indicate that the mass of a putative DM halo must be significantly less than the mass of the stellar component within the observable extent of the cluster. However, given the compact nature and extreme central density of M15, this constraint is not a significant limitation on the potential DM annihilation signal, as evident from the following estimates.

Consider a hypothetical halo model for M15 parameterized by a virial mass m_{vir} and

concentration parameter c. The virial mass is unlikely to be significantly less than estimates of the present baryonic mass of the cluster of $\sim 5 \times 10^5$ M$_\odot$ (Dull et al. 1997; McNamara et al. 2004). Conversely, because of its distance from the Milky Way, the halo mass can not be significantly greater than $\sim 10^8$ M$_\odot$, or dynamical friction would have resulted in the inspiral of the cluster in less than a Hubble time. Based on these constraints, we adopt a range for m_{vir} of 5×10^6 M$_\odot$–5×10^7 M$_\odot$ and consequently a range for c of 32–82 as estimated with the Bullock et al. (2001) relationship, Equation 5. Although the $c(m_{vir})$ correlation was derived with simulated halos of mass $\sim 10^{11}$–10^{14}, Colín et al. (2004) have found that this relationship holds for simulated halos with masses down to $\sim 10^7$ M$_\odot$. To account for tidal disruption due to the interaction with the Milky Way, we truncate the hypothetical model of the DM profile at the optical extent of the cluster, ~ 30 pc.

For the adopted ranges of m_{vir} and c, we estimate J to be 7–150 if the DM halo follows an NFW profile. However, the adiabatic compression of DM in the core of M15 could further enhance the annihilation signal by several orders of magnitude. Simulations by Mashchenko & Sills (2005b) of a two-component globular cluster with stars and DM have demonstrated an enhancement to the central DM density as the baryonic mass profile becomes more centrally concentrated through two-body interactions. To evaluate the enhancement to the central DM density for our hypothetical model of M15, we have used the adiabatic compression model of Blumenthal et al. (1986). With the assumption that the DM travels on circular orbits, this model relates the initial and final baryon and DM mass profiles by the equation,

$$[M_{DM,i}(r_i) + M_{b,i}(r_i)]\, r_i = [M_{DM,f}(r_f) + M_{b,f}(r_f)]\, r_f. \tag{8}$$

The initial distribution of DM is described by an NFW profile parameterized by m_{vir} and c, while the initial baryonic mass profile is assumed to follow the DM mass profile with the cosmological baryon-to-DM ratio of 0.2, following the assumption that globular clusters are among the oldest gravitationally bound systems with cores that have not been significantly influenced by merger events during their evolution. For the final baryonic mass distribution, we adopt a cored profile with $(\alpha,\beta,\gamma) = (2,2.6,0)$, $r_c = 0.04$ pc, and $\rho_s \sim 10^7$ M$_\odot$ pc^{-3} which approximates the nonparametric stellar mass profile presented in Gebhardt et al. (1997). The predicted profile after adiabatic compression, hereafter denoted as NFW+AC, is shown in Figure 7 for the case of $m_{vir} = 10^7$ M$_\odot$ and $c = 50$. The density of DM interior to ~ 10 pc is enhanced by a factor ~ 10–10^2 resulting in an increase in J of $\gtrsim 10^2$. The truncation of the DM halo at 30 pc has a negligible effect on the total annihilation signal. Figure 8 illustrates the scaling of J with the assumed virial mass and concentration of the DM halo. The range of J for the models with and without adiabatic compression are summarized in Table 3.

5.3.   M32

The stellar surface brightness profile of M32 is characterized by a bulge with a half-light radius of 100 pc and a faint surface brightness excess beyond 300 pc which could be interpreted as the remnant of a tidally stripped disk (Graham 2002). A V-band M/L of 2.51 interior to ∼50 pc (van der Marel et al. 1998) is consistent with the expectations of an intermediate age stellar population. Due to the absence of a significant disk component, the available kinematical data do not constrain the presence of an extended DM halo in this system. Its proximity to M31 has lead to speculation that M32 may be the remnant of a normal elliptical or late-type spiral galaxy which was tidally stripped as it passed through the disk of M31 (Bekki et al. 2001; Choi et al. 2002). The extent to which tidal interactions may have stripped the DM halo in this event is unclear.

The mass of the M32 DM halo can be estimated under the hypothesis that its progenitor was a late-type spiral by using the correlation between bulge velocity dispersion σ_c and maximum circular velocity v_c presented by Ferrarese (2002) for a sample of nearby spiral galaxies. Ferrarese (2002) notes that v_c may be related to the virial mass of the DM halo, m_{vir}, using the correlation between them observed for simulated halos by Bullock et al. (2001). By combining these two correlations the following relation between the bulge velocity dispersion and DM halo mass is obtained:

$$\frac{m_{vir}}{10^{12}M_\odot} \sim 5.6 \left(\frac{\sigma_c}{200 \text{ km/s}} \right)^{2.79}. \tag{9}$$

The average bulge velocity dispersion in M32 of 76 ± 10 km s^{-1} (van der Marel et al. 1998) suggests a virial halo mass of 2.5–5×10^{11} M$_\odot$. By further assuming that the DM halo of M32 follows an NFW or Burkert profile, the scale radius and normalization of the halo are fixed by a choice of the concentration parameter c, predicted to be in the range 10–20 by Equation 5. Constraints on the parameters for both NFW and Burkert DM density profiles are plotted in Figure 9. The estimated range of J for these mass models is found to be 1–10 (see Table 3). The models with the range of m_{vir} and c considered here are compatible with the the observed M/L in the interior of M32.

With its extreme central density of 10^7 M$_\odot$ pc^{-3} and two-body core relaxation time of 2–3 Gyr, M32 could possess an enhanced DM cusp produced through the compression of its DM density profile by baryonic infall and the growth of the central black hole. However, it is likely that M32 has undergone multiple mergers during its evolutionary history which could have significantly altered the DM density profile. The degree to which these effects may deplete the central density of DM in this system is uncertain, and therefore the estimate of J obtained with the adiabatic compression model should be considered an upper bound. We

constructed an adiabatic compression model using the same method applied in the case of M15. The initial and final DM and baryon mass profiles for the case of $m_{vir} = 4 \times 10^{11}$ M$_\odot$ and $c = 13.7$ are shown in Figure 10. The range for J for the NFW and NFW+AC models is presented in Table 3.

5.4. M33

M33 is a late-type Sc galaxy with a substantial fraction of its baryonic mass in the form of neutral hydrogen. Measurements of its rotation curve imply a lower limit for the mass of its dark halo of 5×10^{10} M$_\odot$ (Corbelli & Salucci 2000). Corbelli (2003) have modeled the rotation curve, as derived from high-resolution velocity maps of CO, using a three-component density profile which includes a stellar nucleus of $\sim 8 \times 10^8$ M$_\odot$ interior to ~ 0.5 kpc, an exponential disk of mass $\sim 3 \times 10^9$ M$_\odot$, and an extended DM halo with a scale radius ~ 20 kpc. The data is inconsistent with a DM profile with an intermediate power-law asymptotic as steep as r$^{-1.5}$ as proposed by Moore et al. (1999) but can be well matched by either a Burkert or NFW profile. The best-fit region in the (ρ_s, r_s) plane for both NFW and Burkert profiles is shown in Figure 11. Ranges for J derived from the mass models of Corbelli (2003) are presented in Table 3.

Observations of the core of M33 have shown evidence for a stellar nucleus with an effective radius of ~ 3 pc (Lauer et al. 1998; Stephens & Frogel 2002) and a central velocity dispersion of ~ 24 km s^{-1} (Gebhardt et al. 2001). The exceptionally low velocity dispersion in this region sets an upper limit on the mass of a central black hole at $\sim 1.5 \times 10^3$ M$_\odot$ and is compatible with a relaxation timescale of $\sim 10^6$ yr at 0.1 pc. Due to the unusually rapid evolutionary timescale in the stellar nucleus, M33 may be able to sustain a steep DM cusp in its core as DM could be rapidly replenished after a merger or accretion event. The kinematics of this region would be conducive to the growth of an intermediate mass black hole with a relatively large initial to final BH mass ratio and the creation of a DM cusp in the vicinity of the BH. The nucleus of M33 hosts the most luminous steady X-ray source in the local group which is also associated with a radio source and similar to the galactic microquasar GRS 1915+105 (Dubus & Rutledge 2002). A small but significant time variability of 10% in the X-ray luminosity and associated variability in spectral shape have also been observed (La Parola et al. 2003). These data could be interpreting as supporting the existence of an accreting BH in the nucleus of M33. However, the exact enhancement to J through these processes is difficult to estimate given the unknown merger history and therefore an upper bound for J is not presented.

Table 3.   A summary of estimates of J for each source

Source	Distance (kpc)	Model	J_{min}	J_{max}
Draco	80	Burkert	1	10
		NFW	4	40
Ursa Minor	66	NFW	4	20
M15	10	NFW	7	150
		NFW+AC	8×10^3	2×10^4
M32	776	Burkert	0.6	9
		NFW	1	9
		NFW+AC	2×10^5	10^6
M33	840	Burkert	0.03	0.2
		NFW	0.2	0.6

Note. — The contribution of DM substructure may potentially enhance the estimates of J shown here by a factor $\gtrsim 2$ and $\lesssim 100$ as discussed in Section 3.1.

6. Limits on SUSY Parameter Space

For the prediction of gamma-ray fluxes from neutralino self-annihilation, the framework of the minimal supersymmetric extension to the standard model (MSSM) was used. With several simplifying assumptions, the MSSM can be reduced to the seven parameters μ, M_2, $\tan\beta$, m_A, m_q, A_t, and A_b. Random scans of these parameters were performed utilizing the `DarkSUSY` code (Gondolo et al. 2005), and, for each model, the mass m_χ, $\langle\sigma v\rangle$, and relic density $\Omega_{DM}h^2$ of the neutralino were calculated. MSSM models consistent with the ± 3 standard deviation bounds on $\Omega_{DM}h^2$ measured by WMAP (Spergel et al. 2007) were selected for comparison with the derived limits on $\langle\sigma v\rangle$. Figure 12 shows a projection in the $\langle\sigma v\rangle$–m_χ plane of MSSM models that satisfy both the WMAP constraint and the bounds placed by accelerator experiments. The majority of the models with neutralino mass above 100 GeV are concentrated in the band with typical $\langle\sigma v\rangle \lesssim 3 \times 10^{-26}$ cm^3 s^{-1} and extending to $m_\chi \sim 2$ TeV.

For a typical choice of MSSM model parameters, the self-annihilation will predominantly proceed through some combination of the final states $b\bar{b}$, $t\bar{t}$, W^+W^-, or ZZ. The gamma-ray spectra of these channels are similar since they all result from the decay of neutral pions produced in the hadronization of the annihilation products. The $\tau^+\tau^-$ channel produces a significantly harder spectrum as discussed in Section 3.2. Although a neutralino which annihilates predominantly to the $\tau^+\tau^-$ channel would improve the prospects for detection by an ACT, for the MSSM models considered here, the branching fraction of this channel is never more than $\sim 10\%$. Three spectra generated using the `PYTHIA` Monte Carlo code were adopted to cover the possible range of $dN(E, m_\chi)/dE$: the $b\bar{b}$ spectrum, the $\tau^+\tau^-$ spectrum, and a composite spectrum with $BR(\chi\chi \to b\bar{b}) = 0.9$ and $BR(\chi\chi \to \tau^+\tau^-) = 0.1$.

Table 4.   Upper limits on $\langle\sigma v\rangle$ of the neutralino

Source	J	95% C.L. Upper Limit on $\langle\sigma v\rangle$ for $m_\chi = 1$ TeV (cm^3 s^{-1}) $b\bar{b}$	$\tau^+\tau^-$
Draco	13	$< 1.9 \times 10^{-21}$	$< 1.2 \times 10^{-22}$
Ursa Minor	9	$< 3.9 \times 10^{-21}$	$< 2.5 \times 10^{-22}$
M32	3	$< 1.2 \times 10^{-20}$	$< 8.0 \times 10^{-22}$
M33	0.4	$< 8.0 \times 10^{-20}$	$< 5.2 \times 10^{-21}$
M15	32	$< 5.1 \times 10^{-21}$	$< 3.3 \times 10^{-22}$

Following Equation 2, the upper limit on $\langle\sigma v\rangle$ as a function of m_χ for a source with an astrophysical enhancement factor J and an upper limit on the detected rate of gamma rays R_γ (95% C.L.) is given by

$$\left(\frac{\langle\sigma v\rangle}{3\times 10^{-26}\ \text{cm}^3\ \text{s}^{-1}}\right) < R_\gamma\ (95\%\ \text{C.L.})\left(\frac{m_\chi}{100\ \text{GeV}}\right)^2\frac{1.45\times 10^4}{J}$$
$$\times\left[\phi_{1\%}\int_0^\infty A(E)\left(\frac{dN(E,m_\chi)/dE}{10^{-2}\ \text{GeV}^{-1}}\right)dE\right]^{-1},\tag{10}$$

where the assumed form of neutralino annihilation spectrum is convolved with the energy-dependent effective area of the Whipple 10m telescope, $A(E)$, shown in Figure 2. Table 4 presents limits on $\langle\sigma v\rangle$ derived for a neutralino of mass 1 TeV annihilating through the $b\bar{b}$ and $\tau^+\tau^-$ channels. Figure 12 shows the limits on $\langle\sigma v\rangle$ as a function of m_χ for the NFW mass models of Draco and Ursa Minor and the adiabatic compression model (NFW+AC) of M15. Because the effective area of the Whipple 10m telescope rapidly declines below $\sim$400 GeV, the limits on $\langle\sigma v\rangle$ are most constraining for neutralino masses above this energy as discussed in Section 4.2.

Using the most conservative estimates for J, the limits on $\langle\sigma v\rangle$ are 10^4–10^5 times greater than the range predicted for the MSSM models considered in this analysis. The DM mass models of Draco and Ursa Minor have the best observational constraints and the fewest uncertainties with regard to the unknown influence of baryonic matter and merging history. The lower limit on J for these galaxies is relatively insensitive to the assumption of a cusped versus cored DM density profile. The astrophysical contribution to the gamma-ray luminosity could be significantly enhanced if the effects of substructure or a density profile with an inner logarithmic slope > 1 were considered. Limits derived from ACT data on $\langle\sigma v\rangle$ and the monoenergetic line component $\langle\sigma v\rangle_{\gamma\gamma}$ have previously been reported for observations of the G.C. (Aharonian et al. 2006) and M31 (Aharonian et al. 2003; Lavalle et al. 2006). The limits reported by the H.E.S.S. collaboration derived from observations of the G.C. are among the most constraining with a 99% C.L. upper limit on $\langle\sigma v\rangle$ of 10^{-24}–10^{-23}. However these measurements come with a significant systematic uncertainty as they depend sensitively on the accurate modeling of the astrophysical background. For neutralino masses below 100 GeV, EGRET data have also been shown to constrain $\langle\sigma v\rangle$ assuming a range of models for the distribution of DM in substructures and the distribution of substructures in the Milky Way halo (Pieri et al. 2007).

In order for the neutralino to be detectable by the Whipple 10m telescope, a significant enhancement of the DM density is required. Such enhancement may be consistent with the kinematics of M15, M32, and M33. Among the scenarios discussed, the adiabatic compression model for M15 provides the most quantitative estimate for J. In the potentially extreme

DM enhancement scenarios which may exist in M32 and M33, current limits on the gamma-ray rate from these sources already have the potential to constrain the parameter space of allowed SUSY models. If one assumes that DM is composed of neutralinos with $\langle \sigma v \rangle \simeq 3 \times 10^{-26}$ cm^3 s^{-1} and $m_\chi \gtrsim 400$ GeV, then the limits presented in this work rule out a value of J for these sources in excess of $\sim 10^6$.

7. Conclusions

We have conducted a search for the gamma-ray signature of neutralino self-annihilation from five sources: the dwarf spheroidal galaxies Draco and Ursa Minor, the globular cluster M15, and the local group galaxies M32 and M33. Each of these sources was chosen as a favorable representative of different astrophysical conditions that could potentially enhance the neutralino density and gamma-ray self-annihilation flux. For a generic MSSM model of the neutralino, the self-annihilation flux is only detectable by the Whipple 10m telescope if such an enhancement is significant.

A standard analysis of the data revealed no significant excesses, and upper limits on the gamma-ray flux from each source were derived relative to the flux of the Crab Nebula. We have derived limits on $\langle \sigma v \rangle$ of the neutralino as a function of its mass using models for the DM profile of each source and the generic differential gamma-ray spectrum of the neutralino self-annihilation constructed from two representative channels, $b\bar{b}$ and $\tau^+ \tau^-$. Using the upper limit on the gamma-ray rate measured from Draco and the most conservative estimate of the DM distribution in this source, we obtain 95 % C.L. upper limits on $\langle \sigma v \rangle$ of $< 1.9 \times 10^{-21}$ cm^3 s^{-1} and $< 1.2 \times 10^{-22}$ cm^3 s^{-1} for a neutralino of mass 1 TeV annihilating exclusively through the $b\bar{b}$ and $\tau^+ \tau^-$ channels, respectively.

We have considered potential enhancements to the DM self-annihilation flux including the effects of DM substructure and the adiabatic compression of the DM halo due to baryonic infall. These scenarios could enhance the annihilation flux by as much as 10^4 and possibly higher. However the uncertainties of these estimates are large due to the poorly understood dynamics in the cores of the objects as well as their potentially complex merging histories. If one assumes that DM is composed of neutralinos with $\langle \sigma v \rangle \simeq 3 \times 10^{-26}$ cm^3 s^{-1}, then some extreme enhancement scenarios for M32 and M33 may be ruled out.

The current generation of ACTs such as VERITAS, H.E.S.S., MAGIC, and CANGAROO-III have the potential to improve significantly the sensitivity of these measurements and thus probe a larger region of the MSSM parameter space. For a source with a Crab Nebula-like spectrum, VERITAS has a flux sensitivity ~ 10 times better than the Whipple 10m telescope

and a peak detection rate near 150 GeV. The lower energy threshold of VERITAS will allow it to be sensitive to the low to intermediate neutralino mass range of 100 GeV–1 TeV. With the improved sensitivity of these instruments, conventional astrophysical backgrounds may become significant. The sensitivity of observations of the G.C. to DM annihilations is already limited by the presence of such backgrounds. Observations of extragalactic sources such as those discussed in this work have the potential to avoid this limitation. Furthermore, the identification of the unique spectral signature of DM self-annihilations in two or more of these sources would effectively rule out a traditional astrophysical process. Next-generation ACT instruments such as the currently planned Cherenkov Telescope Array (CTA) and Advanced Gamma Ray Imaging System (AGIS) will potentially be 10^2–10^3 times as sensitive as the Whipple 10m telescope and could perform dedicated deep observations with 10–10^2 times longer exposure than the observations presented in this work. This may allow the exclusion of MSSM models with even the most conservative assumptions for the DM distribution in the sources with the lowest anticipated astrophysical backgrounds such as the dwarf spheroidal galaxies.

REFERENCES

Aharonian, F. et al. 2006, Physical Review Letters, 97, 221102

Aharonian, F., & Neronov, A. 2005, ApJ, 619, 306

Aharonian, F. A. et al. 2004, A&A, 425, L13

—. 2003, A&A, 400, 153

Albert, J. et al. 2006, ApJ, 638, L101

Aparicio, A., Carrera, R., & Martínez-Delgado, D. 2001, AJ, 122, 2524

Atoyan, A., & Dermer, C. D. 2004, ApJ, 617, L123

Bahcall, J. N., & Wolf, R. A. 1976, ApJ, 209, 214

Baltz, E. A., Briot, C., Salati, P., Taillet, R., & Silk, J. 2000, Phys. Rev. D, 61, 023514

Bekki, K., Couch, W. J., Drinkwater, M. J., & Gregg, M. D. 2001, ApJ, 557, L39

Bellazzini, M., Ferraro, F. R., Origlia, L., Pancino, E., Monaco, L., & Oliva, E. 2002, AJ, 124, 3222

Bergström, L., & Hooper, D. 2006, Phys. Rev. D, 73, 063510

Bergström, L., & Ullio, P. 1997, Nuclear Physics B, 504, 27

Bergström, L., Ullio, P., & Buckley, J. H. 1998, Astroparticle Physics, 9, 137

Binney, J., & Tremaine, S. 1987, Galactic dynamics (Princeton, NJ, Princeton University Press, 1987, 747 p.)

Birkedal, A., Matchev, K. T., Perelstein, M., & Spray, A. 2005, ArXiv High Energy Physics - Phenomenology e-prints

Blumenthal, G. R., Faber, S. M., Flores, R., & Primack, J. R. 1986, ApJ, 301, 27

Bottino, A., Donato, F., Fornengo, N., & Scopel, S. 2003, Phys. Rev. D, 68, 043506

Bullock, J. S., Kolatt, T. S., Sigad, Y., Somerville, R. S., Kravtsov, A. V., Klypin, A. A., Primack, J. R., & Dekel, A. 2001, MNRAS, 321, 559

Burkert, A. 1995, ApJ, 447, L25+

Choi, P. I., Guhathakurta, P., & Johnston, K. V. 2002, AJ, 124, 310

Clowe, D., Bradač, M., Gonzalez, A. H., Markevitch, M., Randall, S. W., Jones, C., & Zaritsky, D. 2006, ApJ, 648, L109

Colafrancesco, S., Profumo, S., & Ullio, P. 2007, Phys. Rev. D, 75, 023513

Colín, P., Klypin, A., Valenzuela, O., & Gottlöber, S. 2004, ApJ, 612, 50

Corbelli, E. 2003, MNRAS, 342, 199

Corbelli, E., & Salucci, P. 2000, MNRAS, 311, 441

Corbin, M. R., O'Neil, E., & Rieke, M. J. 2001, AJ, 121, 2549

de Blok, W. J. G., McGaugh, S. S., Bosma, A., & Rubin, V. C. 2001, ApJ, 552, L23

del Burgo, C., Peletier, R. F., Vazdekis, A., Arribas, S., & Mediavilla, E. 2001, MNRAS, 321, 227

Diemand, J., Kuhlen, M., & Madau, P. 2006, ApJ, 649, 1

—. 2007, ApJ, 657, 262

Diemand, J., Zemp, M., Moore, B., Stadel, J., & Carollo, M. 2005, MNRAS, 364, 665

Dubus, G., & Rutledge, R. E. 2002, MNRAS, 336, 901

Dull, J. D., Cohn, H. N., Lugger, P. M., Murphy, B. W., Seitzer, P. O., Callanan, P. J.,
     Rutten, R. G. M., & Charles, P. A. 1997, ApJ, 481, 267

Eskridge, P. B., & Schweitzer, A. E. 2001, AJ, 122, 3106

Ferrarese, L. 2002, ApJ, 578, 90

Gebhardt, K. et al. 2001, AJ, 122, 2469

Gebhardt, K., Pryor, C., Williams, T. B., Hesser, J. E., & Stetson, P. B. 1997, AJ, 113, 1026

Gnedin, O. Y., Kravtsov, A. V., Klypin, A. A., & Nagai, D. 2004, ApJ, 616, 16

Gondolo, P., Edsjö, J., Ullio, P., Bergstrom, L., Schelke, M., & Baltz, E. A. 2005, New
     Astronomy Review, 49, 149

Gondolo, P., & Silk, J. 1999, Physical Review Letters, 83, 1719

Graham, A. W. 2002, ApJ, 568, L13

Green, A. M., Hofmann, S., & Schwarz, D. J. 2005, Journal of Cosmology and Astro-Particle
     Physics, 8, 3

Griest, K., & Kamionkowski, M. 1990, Physical Review Letters, 64, 615

Helene, O. 1983, Nuclear Instruments and Methods in Physics Research A, 212, 319

Hillas, A. M. 1985, in International Cosmic Ray Conference, ed. F. C. Jones, 445–448

Hillas, A. M. et al. 1998, ApJ, 503, 744

Horns, D. 2005, Physics Letters B, 607, 225

Joseph, C. L. et al. 2001, ApJ, 550, 668

Jungman, G., Kamionkowski, M., & Griest, K. 1996, Phys. Rep., 267, 195

Kildea, J. et al. 2007, in press, Astroparticle Physics, 10.1016/j.astropartphys.2007.05.004

Kleyna, J. T., Wilkinson, M. I., Gilmore, G., & Evans, N. W. 2003, ApJ, 588, L21

Kosack, K. et al. 2004, ApJ, 608, L97

La Parola, V., Damiani, F., Fabbiano, G., & Peres, G. 2003, ApJ, 583, 758

Lauer, T. R., Faber, S. M., Ajhar, E. A., Grillmair, C. J., & Scowen, P. A. 1998, AJ, 116, 2263

Lavalle, J. et al. 2006, A&A, 450, 1

Li, T.-P., & Ma, Y.-Q. 1983, ApJ, 272, 317

Mashchenko, S., & Sills, A. 2005a, ApJ, 619, 243

—. 2005b, ApJ, 619, 258

Mashchenko, S., Sills, A., & Couchman, H. M. 2006, ApJ, 640, 252

McNamara, B. J., Harrison, T. E., & Baumgardt, H. 2004, ApJ, 602, 264

Merritt, D., & Cruz, F. 2001, ApJ, 551, L41

Merritt, D., Ferrarese, L., & Joseph, C. L. 2001, Science, 293, 1116

Merritt, D., Graham, A. W., Moore, B., Diemand, J., & Terzić, B. 2006, AJ, 132, 2685

Milosavljević, M., Merritt, D., Rest, A., & van den Bosch, F. C. 2002, MNRAS, 331, L51

Moore, B. 1996, ApJ, 461, L13+

Moore, B., Quinn, T., Governato, F., Stadel, J., & Lake, G. 1999, MNRAS, 310, 1147

Muñoz, R. R. et al. 2005, ApJ, 631, L137

Navarro, J. F., Frenk, C. S., & White, S. D. M. 1996, ApJ, 462, 563

Navarro, J. F. et al. 2004, MNRAS, 349, 1039

Peebles, P. J. E. 1984, ApJ, 277, 470

Piatek, S., Pryor, C., Armandroff, T. E., & Olszewski, E. W. 2002, AJ, 123, 2511

Pieri, L., Bertone, G., & Branchini, E. 2007, ArXiv e-prints, 706

Reynolds, P. T. et al. 1993, ApJ, 404, 206

Saitoh, T. R., Koda, J., Okamoto, T., Wada, K., & Habe, A. 2006, ApJ, 640, 22

Ségall, M., Ibata, R. A., Irwin, M. J., Martin, N. F., & Chapman, S. 2007, MNRAS, 1503

Shetrone, M. D., Côté, P., & Sargent, W. L. W. 2001, ApJ, 548, 592

Sjöstrand, T., Edén, P., Friberg, C., Lönnblad, L., Miu, G., Mrenna, S., & Norrbin, E. 2001, Computer Physics Communications, 135, 238

Spergel, D. N. et al. 2007, ApJS, 170, 377

Stephens, A. W., & Frogel, J. A. 2002, AJ, 124, 2023

Strigari, L. E., Koushiappas, S. M., Bullock, J. S., & Kaplinghat, M. 2007, Phys. Rev. D, 75, 083526

Tegmark, M. et al. 2004, Phys. Rev. D, 69, 103501

Tyler, C. 2002, Phys. Rev. D, 66, 023509

Ullio, P., Zhao, H., & Kamionkowski, M. 2001, Phys. Rev. D, 64, 043504

van den Bosch, R., de Zeeuw, T., Gebhardt, K., Noyola, E., & van de Ven, G. 2006, ApJ, 641, 852

van der Marel, R. P., Cretton, N., de Zeeuw, P. T., & Rix, H.-W. 1998, ApJ, 493, 613

Weekes, T. C. 1996, Space Science Reviews, 75, 1

Wilkinson, M. I., Kleyna, J. T., Evans, N. W., Gilmore, G. F., Irwin, M. J., & Grebel, E. K. 2004, ApJ, 611, L21
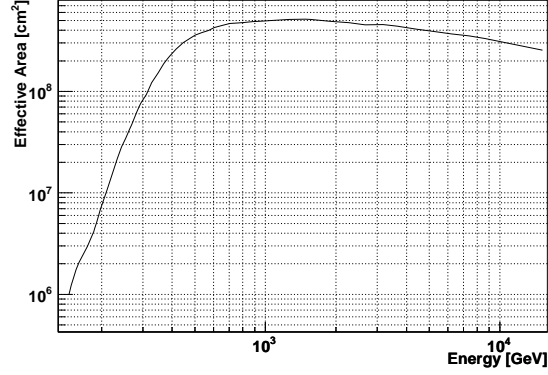
Fig. 2.— Effective area of the Whipple 10m telescope as a function of energy after selection of gamma-ray-like events with the *Supercuts* criteria. The effective area below 150 GeV was assumed to be 0 in all computations.
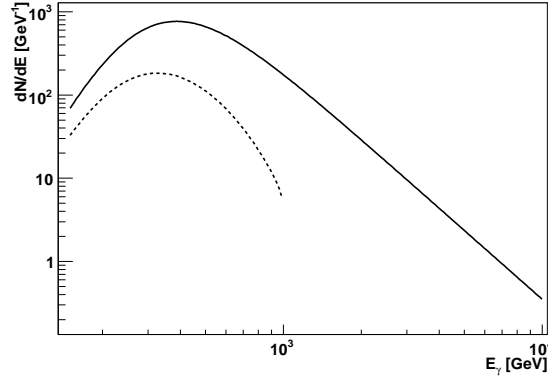
Fig. 3.— Comparison of the differential detection rate of the Crab Nebula (solid line) and a DM halo with $\langle \sigma v \rangle = 3 \times 10^{-26}$, $m_\chi = 1$ TeV, and $J = 10^6$ (dashed line). The *Supercuts* selection criteria are used.
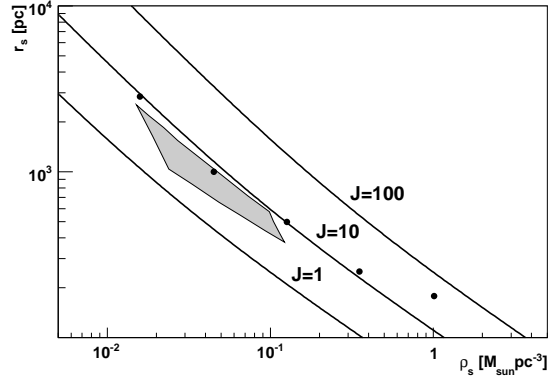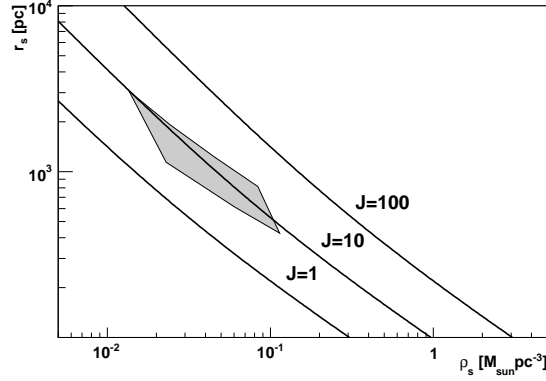
Fig. 4.— Constraints from stellar kinematics data on the parameters r_s and ρ_s of the Draco DM halo under the assumption of an NFW profile. The gray contour and solid circles indicate the best-fit mass models of Strigari et al. (2007) and Mashchenko et al. (2006), respectively. The parameters r_s and ρ_s are defined for the NFW and Burkert halo profiles in Equations 4 and 6.
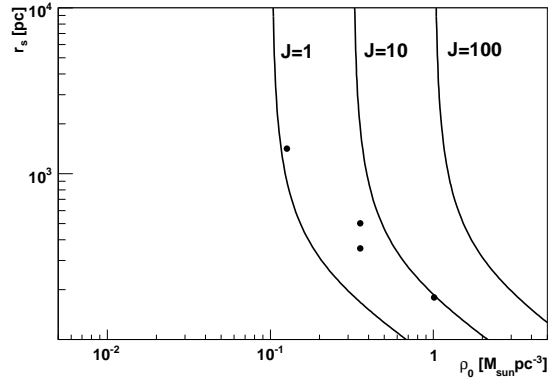
Fig. 5.— Constraints from stellar kinematics data on the parameters r_s and ρ_s of the Draco DM halo under the assumption of a Burkert profile. The solid circles indicate the best-fit mass models of Mashchenko et al. (2006). Thick solid lines indicate contours of constant J.

Fig. 6.— Constraints from stellar kinematics data on the parameters r_s and ρ_s of the Ursa Minor DM halo under the assumption of an NFW profile. The grey contour indicates the best-fit mass models of Strigari et al. (2007). Thick solid lines indicate contours of constant J.
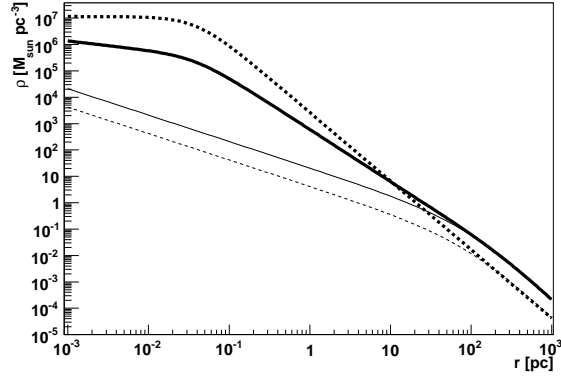

Fig. 7.— Shown is the M15 DM density profile before (thin solid line) and after (thick solid line) adiabatic compression modeled as described in the text. Thin and thick dashed lines show the same comparison for the baryonic density profile.
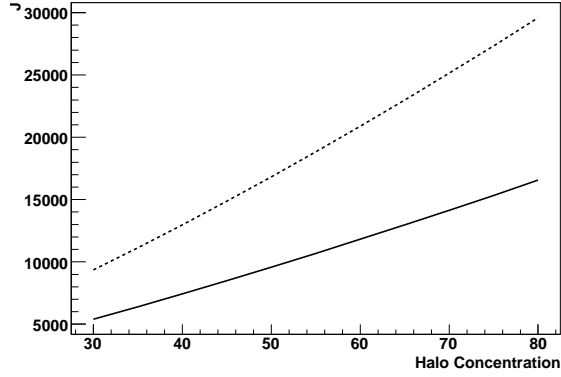
Fig. 8.— J for the NFW+AC model of M15 as a function of the concentration parameter of the initial DM halo. The solid and dashed lines show the scaling for a DM halo of total virial mass 5×10^6 M$_\odot$ and 5×10^7 M$_\odot$ respectively.
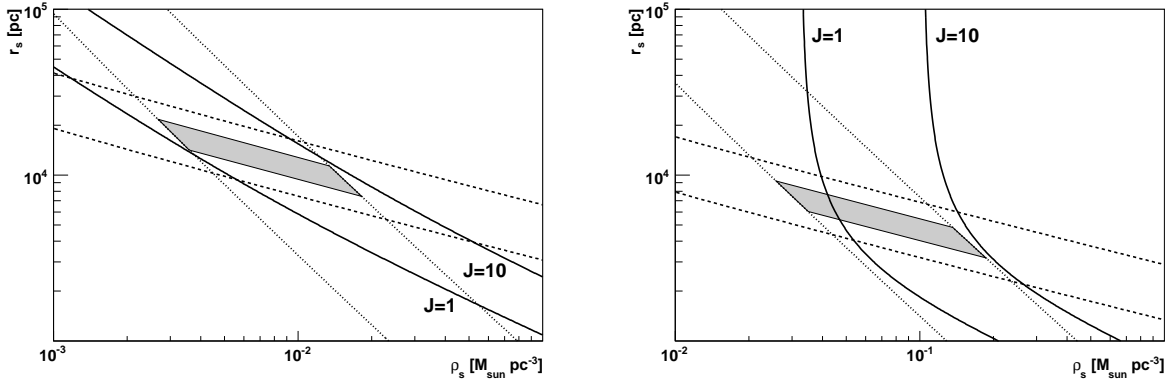

Fig. 9.— Constraints derived using Equations 9 and 5 for M32 on the parameters r_s and ρ_s of its DM halo under the assumption of an NFW (left panel) and Burkert (right panel) profile. Dashed lines show contours of constant virial mass for 10^{11} M$_\odot$ (lower) and 10^{12} M$_\odot$ (upper). Dotted lines denote the ± 1 standard deviation bounds on the median halo concentration to virial mass relation, Equation 5. Thick solid lines indicate contours of constant J.
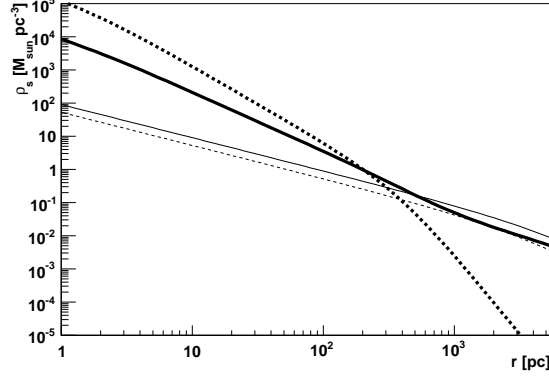
Fig. 10.— A comparison for M32 of the stellar density profile of van der Marel et al. (1998) (thick dashed line) with the modeled DM density profiles before (thin solid line) and after (thick solid line) adiabatic compression. The thin dashed line shows the assumed initial baryonic density profile.
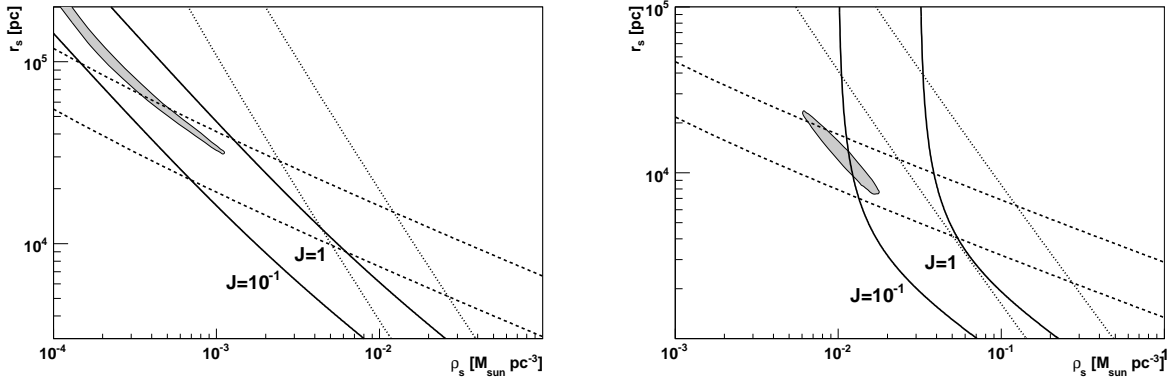

Fig. 11.— Constraints from CO rotation curve data for M33 on the parameters r_s and ρ_s of its DM halo under the assumption of an NFW (left panel) and Burkert (right panel) profile. The gray-shaded region indicates the 3 standard deviation constraints reported by Corbelli (2003). Dashed lines show contours of constant virial mass for 10^{11} $M_\odot$ (lower) and 10^{12} $M_\odot$ (upper). Dotted lines denote the ± 1 standard deviation bounds on the median halo concentration to virial mass relation, Equation 5. Thick solid lines indicate contours of constant J.
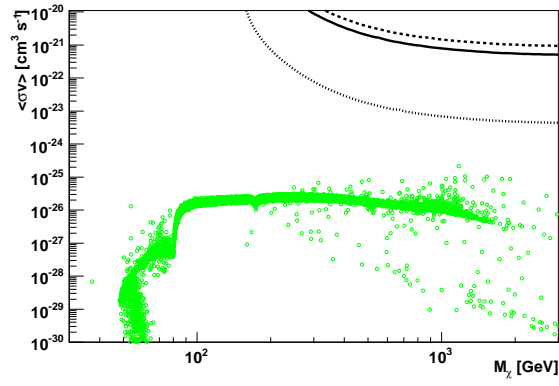
Fig. 12.— Upper limits on $\langle \sigma v \rangle$ as a function of m_χ calculated using Equation 10 with a composite neutralino spectrum and the J values obtained for the Draco (solid line) and Ursa Minor (dashed line) NFW models and the M15 NFW+AC model (dotted line). Shown as open circles are MSSM models that fall within ± 3 standard deviations of the relic density measured in the three-year WMAP data set (Spergel et al. 2007).